Applied Catalysis A, General 660 (2023) 119185

Contents lists available at ScienceDirect

Applied Catalysis A, General

journal homepage: www.elsevier.com/locate/apcata

Tuning the hydrogenation of CO_2 to CH_4 over mechano-chemically prepared palladium supported on ceria

Maila Danielis [a,1], Juan D. Jiménez [b,1], Ning Rui [b], Jorge Moncada [b], Luis E. Betancourt [b], Alessandro Trovarelli [a], José A. Rodriguez [b], Sanjaya D. Senanayake [b,*], Sara Colussi [a,*]

[a] Polytechnic Department, University of Udine and INSTM, Via del Cotonificio 108, 33100 Udine, Italy
[b] Chemistry Division, Brookhaven National Laboratory, Upton, NY, USA

ARTICLE INFO

Keywords:
Direct methanation
Carbon dioxide activation
Dry milling
Pd/CeO_2

ABSTRACT

CO_2 methanation reactivity, reaction mechanism, and surface structure were investigated on a mechanochemically prepared Pd/CeO_2 catalyst ($PdAcCeO_2$-M), where an oxidative pretreatment (-o) increased methane yield by a factor of two compared to a reductive pretreatment (-h). Methanation rates were maintained for over 48 h and further increased upon oxidative regeneration treatments. The surface species of both $PdAcCeO_2$-M-o and $PdAcCeO_2$-M-h were explored via *in situ* CO_2 and CO hydrogenation DRIFTS, where CO hydrogenation effectively models the dissociative CO_2 mechanism ($CO_2 \rightarrow CO \rightarrow CH_4$). $PdAcCeO_2$-M-o yielded distinct Pd-CO adsorption and the absence of monodentate carbonate at ~ 1400 cm^{-1}, while AP-XPS showed that $PdAcCeO_2$-M-o yielded a unique $Pd^{\delta+}$ contribution at 335.9 eV. By gaining insights from various *in situ* spectroscopic techniques, and by breaking the CO_2 hydrogenation mechanism into piecewise steps, a deeper understanding of the direct CO_2 reduction towards methane and CO over mechanochemically prepared Pd/CeO_2 catalysts was obtained.

1. Introduction

As the need to curb carbon dioxide emissions is taking increasing global attention as a means to mitigate climate change, the direct transformation of CO_2 to value added products represents an economically viable approach to carbon fixation [1–3]. Currently, the primary means of upgrading CO_2 into value added products consist of its electrochemical and/or thermo-catalytic conversion [4,5]. The conversion of CO_2 is especially hindered by the exceptional stability of the molecule, which is much higher than any reaction intermediate and thus leads to complex reaction mechanisms. Hence, the selectivity of catalysts for desired CO_2 hydrogenation reaction is of utmost interest. The methanation of CO_2 is a promising approach due to advantages of being able to feed renewable natural gas directly into the existing infrastructure, allowing for facile widescale adoption [6]. Depending on the supported metal [7,8], cluster size [9–12], and metal-support interaction [13–15], the selectivity towards desired products can be obtained: as an example, catalysts containing nickel [16–18], cobalt [12,19–21], and ruthenium [9,22,23] are generally used for the production of methane from CO_2, Pd [24–26] and Cu [27–29] based catalysts for the synthesis of methanol, and olefin production is achieved over Ir or Fe based catalysts using zeolites or mixed metal oxides as supporting materials [30,31]. Palladium is generally used as a promoter for H_2 dissociation, in tandem with materials with poor H_2 dissociation capabilities, such as Cu [32], In_2O_3 [33] or Fe [34], or simply to increase the rate of reaction by decoupling the H_2 activation and CO_2 reaction active sites in bimetallic alloys such as PdCo [35], PdZn [36] or PdNi systems [34]. The use of Pd as a promoter for hydrogenation [37,38] and its interactions with hydrogen are well understood, however, the contributions and chemistry of Pd alone, specifically for CO_2 hydrogenation to CO or CH_4, are less understood.

In addition to modulation of the metal phase, metal support interplays can also be exploited to increase the reactivity of a catalyst for CO_2 hydrogenation [14,15]. In this respect, cerium oxide, CeO_2, is widely used [7,25,39,40], allowing control of the supported particle size thanks to ceria's unique ability to trap adatoms during Ostwald ripening, resulting in highly dispersed, reversible catalysts [9,41] and simultaneously promoting strong metal-support interactions. Oxidative

* Corresponding authors.
E-mail addresses: ssenanay@bnl.gov (S.D. Senanayake), sara.colussi@uniud.it (S. Colussi).
[1] Authors contributed equally.

https://doi.org/10.1016/j.apcata.2023.119185
Received 23 January 2023; Received in revised form 10 March 2023; Accepted 6 April 2023
Available online 7 April 2023

treatments have also shown a unique ability to redisperse noble metals supported on ceria under reaction conditions, increasing activity and promoting the formation of more uniform and selective catalysts for various reactions [42]. Ceria also facilitates closing the catalytic cycle by supplying lattice oxygen, interfacial oxygen vacancies, and redox contributions to facilitate the catalytic exchange for CO_2 hydrogenation [16,43,44].

Ball milling has been recently shown as a promising tool for the generation of novel metal species in close interaction with the support oxide [45,46], resulting in distinct active sites that promote unique catalytic properties [47,48] or enable selective reaction routes [49]. The use of mechanical energy in substitution of conventional solution-based synthesis routes has shown interesting results in the preparation of advanced nanomaterials due to the generation of amorphous or meta-stable phases [50–52] and, more recently, serious efforts have been paid to translate these effects to metal-supported heterogeneous catalysts [47,53,54]. We have shown in recent studies how the mechanical action induces the formation of unique Pd-Ce sites on Pd/CeO_2 catalysts for CO_2 and CH_4 activation [55–57], where the intimate interaction between Pd, Ce and O atoms at the catalyst surface resulted in enhanced catalytic activity and stability for low temperature CH_4 conversion [47,55] and enabled different reaction mechanisms in the dry reforming of methane (DRM) via selective CO_2 activation [56].

Here, we seek to investigate in detail the contribution of these unique Pd-Ce sites in the low temperature hydrogenation of CO_2, evaluating their evolution during reaction. In this study, the mechanism of CO_2 hydrogenation was explored on Pd/CeO_2 samples prepared by mechanochemical synthesis (M) via an array of techniques, including *in situ* DRIFTS and isotopic labeling, ambient pressure XPS, and *ex situ* XRD, for both CO_2 hydrogenation and CO hydrogenation, aiming to discern the influence of both the associative and dissociative CO_2 mechanisms. Over $PdAcCeO_2$-M, an oxidative treatment was observed to uniquely lead to the associative CO_2 hydrogenation pathway, promoting CH_4 selectivity and long-term stability. As revealed by AP-XPS analysis, the observed pathway on the milled sample is facilitated by a partially oxidized $Pd^{\delta+}$ state, thus highlighting novel structure-selectivity relations for the low temperature CO_2 activation.

2. Experimental methods

2.1. Catalysts synthesis

A 4 wt%Pd catalyst supported on CeO_2 was prepared using an optimized mild mechanochemical synthesis method, reported in detail elsewhere [55], using palladium acetate as the Pd precursor ($PdAcCeO_2$-M). In brief, an appropriate amount of commercial CeO_2 support (Rhodia) was calcined in static air at 900 °C for 3 h (BET surface area: 25 m^2/g) before milling with the corresponding amount of $Pd(OAc)_2$ powders (99.9%, Sigma-Aldrich), using a 15 mL ZrO_2 grinding jar and one ZrO_2 milling sphere in a Fritsch Pulverisette P23 mill operating at 15 Hz.

2.2. Catalytic performance evaluation

CO_2 hydrogenation reactions were carried out at atmospheric pressure using a 4:1 ratio of H_2:CO_2 (1% CO_2, 4% H_2, balanced in inert gas) on 150 mg of catalyst, with a total flow rate of 60 mL/min and a GHSV of 48,000 h^{-1}; the catalysts were sieved to 225–180 mesh size to prevent pressure buildup during reaction. Reductive pretreatments were carried out at 400 °C for 30 min under a 4% H_2 balanced in inert feed gas, and oxidative treatments were carried out at 500 °C under synthetic air (21% O_2/N_2) for 1 h; all ramp rates were 10 °C/min and the reactor was cooled to room temperature before reaction. Pretreatment conditions were chosen based on previous studies, reporting significant differences in structure among catalysts [55,56]. The reducing or oxidizing pretreatments are indicated in the following by a suffix -h or -o, respectively, added to the sample name. CO_2 hydrogenation tests were carried out in transient or stationary conditions: temperature ramp tests were carried out heating the sample stepwise from 100° to 500°C, with 20 min isothermal steps every 50 °C, and then ramped back down to close the loop. Stationary time-on-stream tests were performed after the indicated -h or -o pretreatment and brought up to 400 °C under reaction conditions of 1% CO_2, 4% H_2 and balanced in N_2 with an overall space velocity of 48,000 h^{-1}, holding the sample at these conditions for approximately 48 h. Another time-on-stream experiment was carried out after an initial oxygen pretreatment to verify the effect of switching pretreatment atmosphere: first, the sample was held under reaction conditions at 400 °C for approximately 12 h, then a reducing pretreatment (4% H_2/N_2 at 400 °C for 30 min) was performed and the catalyst was switched back to reaction conditions (1% CO_2, 4% H_2 in nitrogen at 400 °C) for an additional 3 h. Afterwards, a secondary oxygen pretreatment at 500 °C for 1 h was performed followed by a return to reaction conditions for the duration of the experiment. Products and reagents during all cycling and stationary experiments were analyzed via an on line GC (Agilent 7980B), equipped with both a TCD and a FID detector, and an MS (SRS 100). CO_2 conversion (X_{CO_2}), CO and CH_4 yield (Y_{CH_4}, Y_{CO}) and selectivity (S_{CH_4}, S_{CO}) were used to evaluate catalytic performance, using the following equations:

$$X_{CO_2}(\%) = \frac{F_{CO_2,in} - F_{CO_2,out}}{F_{CO_2,in}} \bullet 100$$

$$Y_{CO,CH_4}(\%) = \frac{F_{CO,CH_4}}{F_{CO_2,in}} \bullet 100$$

$$S_{CO,CH_4}(\%) = \frac{F_{CO,CH_4}}{F_{CO_2,in} - F_{CO_2,out}} \bullet 100$$

2.3. XRD measurements

XRD analysis was carried out *ex situ* to follow the CeO_2 structure and the evolution of Pd species taking place during reaction. X-Ray diffraction patterns were collected on samples as prepared, after the pretreatment and after reaction, using a Philips X′Pert Diffractometer with an X′Celerator detector using Ni-filtered Cu Kα radiation (λ = 1.542 Å) operating at 40 kV and 40 mA. Full diffractograms were collected in the 20–100° 2θ range (0.02° step size, 40 s counting time per step). Additional measurements were carried out in the 32–48° 2θ range (0.02° step size, 320 s counting time per step) to focus on the palladium peak range. Scherrer's formula was used to estimate the average Pd particle size using the Pd (111) peak at 40.2°:

$$D_{Pd} = \frac{0.9\lambda}{B\cos\theta}$$

where λ is the X-ray wavelength, 0.9 is a correction value for spherical particles, and B corresponds to the FWHM of the peak corrected by the instrumental error.

$$B = \sqrt{B_{obs}^2 - B_{inst}^2}$$

2.4. TGA analysis

Thermogravimetric analysis (TGA) was carried out in a Q500 - TA Instruments to measure the amount of residual carbon after reaction. TGA experiments were carried out under synthetic air (21% O_2/N_2) with a total gas flow of 60 mL/min; ~15 mg of sample were loaded on a platinum pan, then the sample was heated at 10 °C/min from RT to 900 °C and gradually cooled to 100 °C while continuously measuring the weight loss.

2.5. DRIFTS measurements

In situ DRIFTS spectra were collected in Kubelka−Munk (K−M) mode using an FTIR spectrometer (Bruker Vertex 70) equipped with a Harrick Praying Mantis cell, MCT detector, and a mass spectrometer. Samples were pretreated in either 4%H_2/He at 400 °C for 30 min or 21%O_2/He at 500 °C for 1 h. After pretreatment, the samples were cooled down to room temperature and purged with He to remove excess adsorbed gas. Scans were collected at 250 °C and 400 °C by heating the samples at a 10 °C/min ramp rate and holding the temperature in either CO_2 hydrogenation conditions (1%CO_2, 4%H_2, balance He), CO_2 adsorption conditions (1%CO_2 balanced in He) or CO hydrogenation conditions (1%CO, 3%H_2, balance in He). Isotopic labeling was performed using an in-house gas pulsing system coupled with a fast time resolution IR interface scanning every six seconds, where the catalyst was heated up to reaction temperature under inert gas then switched to the CO_2/H_2 feed and allowed to reach steady state for approximately 10 min. After steady state DRIFTS conditions were achieved, indicated by a constant IR absorbance signal of all surface species, the feed was switched to CO_2/D_2 using the same 1:4 ratio of CO_2:D_2 and allowed to run for 10 min to reach steady state under isotopically labeled conditions. Additionally, the cycling between CO_2/H_2 and CO_2/D_2 was carried out an additional ten times to ensure reproducibility in the spectra and the D_2 uptake while spectra were collected every 7 s. Background spectra were collected at the reported temperature before any scan under pure He gas, where the background was allowed to equilibrate for at least 3 consecutive scans before data collection. All spectra have a 4 cm^{-1} spectral resolution.

2.6. Ambient pressure X-ray photoelectron spectroscopy (AP-XPS)

A commercial SPECS AP-XPS chamber equipped with a PHOIBOS 150 EP MCD-9 analyzer at the Chemistry Division of Brookhaven National Laboratory (BNL) was used for XPS analysis [58]. The Ce *3d* photoemission line with the strongest Ce^{4+} feature (916.9 eV) was used for energy calibration. The powder catalyst was pressed on an aluminum plate and then loaded into the AP-XPS chamber. Room temperature scans were collected under UHV conditions while elevated temperature measurements (at 250 °C and 400 °C) were carried out at a 30 mtorr total pressure using a 4:1 gas mixture of H_2:CO_2.

3. Results and discussion

3.1. Catalytic performance

The catalytic performance of PdAcCeO$_2$-M was explored for CO_2 hydrogenation after a reducing or oxidizing treatment, denoted as PdAcCeO$_2$-M-h and PdAcCeO$_2$-M-o, respectively, as a function of temperature, as shown in Fig. 1. Both catalysts show similar CO_2 conversion across all temperatures, however, notable differences in the selectivity toward methane can be observed. In particular, PdAcCeO$_2$-M-o exhibits a higher CH_4 yield compared to PdAcCeO$_2$-M-h at 400 °C, on which CO production is favored, while full selectivity to CO is observed on both samples at low temperature (250 °C). This is corroborated by equilibria calculations for CO, CH_4 and CO_2 considering the methanation and RWGS reactions [59]: the activity of the PdAcCeO$_2$-M sample after reducing pretreatment follows pretty closely the RWGS equilibrium data, as does the sample after oxidizing pretreatment at low (250 °C) temperatures, while a distinct shift to methanation equilibrium values is observed on PdAcCeO$_2$-M-o above 300 °C (Fig. S1).

Likely, by changing the pretreatment conditions we selectively expose distinct active sites, possibly as a consequence of the oxidative atmosphere yielding redispersion of Pd [9]. Indeed, the catalytic activity of the PdAcCeO$_2$-M sample without any pretreatment, where the palladium acetate salt rapidly decomposes to metallic Pd, closely resembles the one obtained after H_2 treatment (Fig. S2). However, the palladium sites obtained after O_2 exposure are not lost during reaction, despite the strongly reducing atmosphere, and the activity was found to be stable over a closed heating/cooling loop test (Fig. S3). The robust nature of the catalysts was also probed via exposing the oxidized PdAcCeO$_2$-M-o to a subsequent reduction step, denoted as PdAcCeO$_2$--M-o-h, which shows that the catalytic performance for CO_2 hydrogenation was preserved without altering methane and CO yield (Fig. S4). A comparison between the catalyst explored herein and other noble metal-based catalysts reported in the literature shows that the reactivity of these materials is consistent with other notable noble and base transition metal catalyst for CO_2 methanation (Table S1).

The stability of the catalytic performance after reducing and oxidative conditions was studied under prolonged time-on-stream tests (Fig. 2), where the selectivity towards CH_4 at 400 °C appears to be stable for over 48 h; only a small deactivation trend can be observed, which might be due to slight sintering of Pd nanoparticles on the catalyst surface. To test the robust nature of the catalyst exposed to oxygen pretreatment, additional intermittent treatments were performed during reaction (Fig. 3): after approximately 12 h of CO_2 hydrogenation

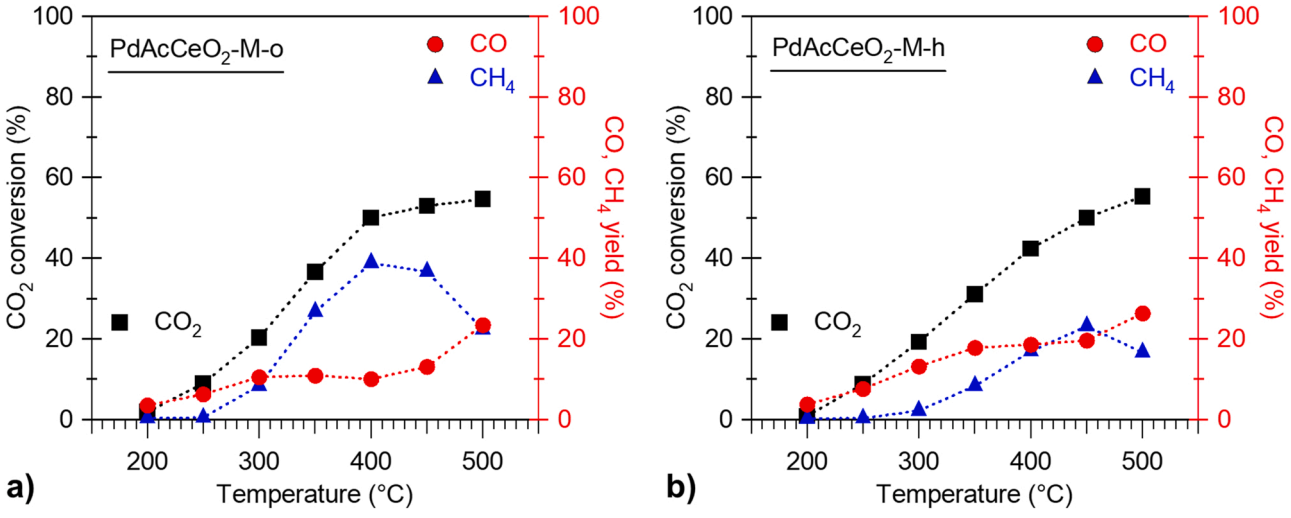

Fig. 1. CO_2 hydrogenation catalytic performance of PdAcCeO$_2$-M after either (a) an oxidative or (b) a reducing pretreatment.

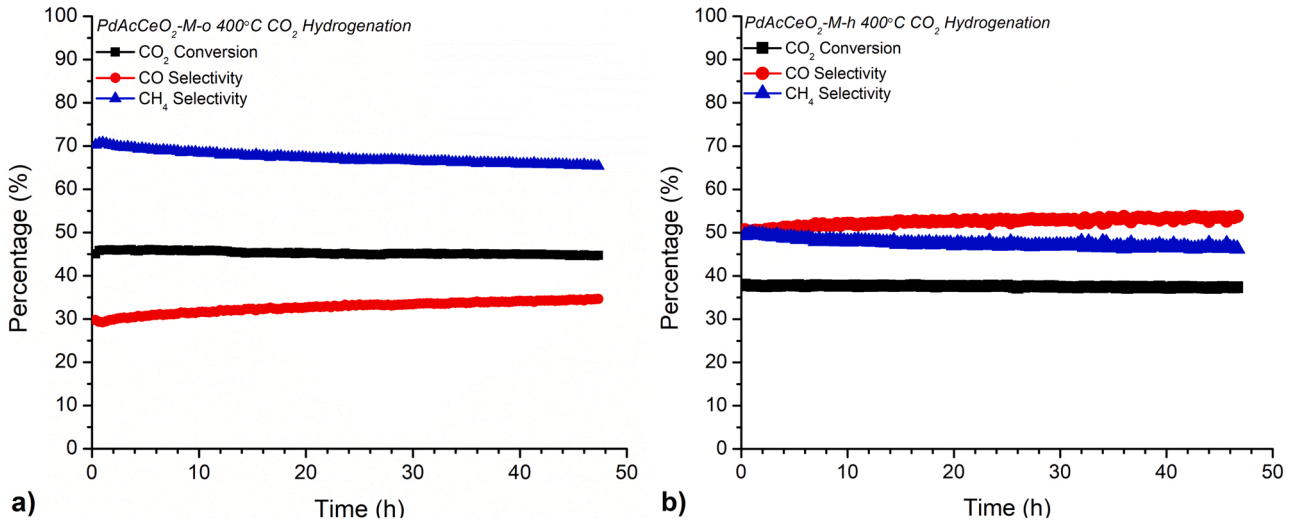

Fig. 2. Time-on-stream catalytic performance for $PdAcCeO_2$-M catalysts after (a) oxidative (21%O_2/N_2, -o) or (b) reducing (4%H_2/N_2, -h) pretreatment conditions. Reaction conditions: 1% CO_2, 4% H_2, balance N_2, 48,000 h^{-1} GHSV, 1 atm pressure, 400 °C.

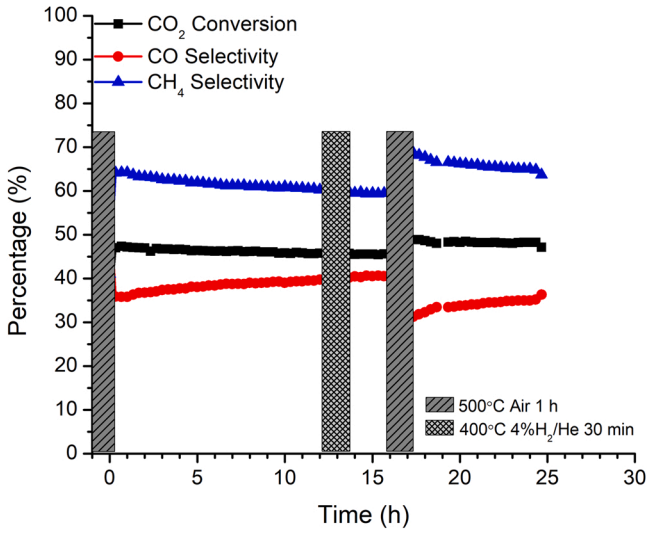

Fig. 3. CO_2 Hydrogenation cycling test after an initial oxidative pretreatment. Reaction conditions: 1%CO_2, 4%H_2, balance N_2, 48,000 h^{-1} GHSV, 1 atm pressure, 400 °C. Cycling conditions: oxidative treatment is 500 °C under air for 1 h and reductive conditions are 400 °C under 4% H_2/He for 30 min.

reaction conditions, a reductive treatment at 400 °C under 4% H_2 for 30 min was performed, however, this did not result in any observable change in reactivity upon switching back to CO_2 hydrogenation conditions. A secondary oxidative pretreatment was carried out after additional 3 h of time on stream, followed by an increase in both CO_2 conversion and CH_4 selectivity, by 5% and 7% respectively, which then remained stable for the whole experiment duration.

3.2. XRD analysis

To investigate the structural evolution of Pd species after the different pretreatment conditions and after exposure to reaction conditions, *ex situ* XRD analysis was carried out. The Pd 2θ patterns collected over $PdAcCeO_2$-M as prepared, after pretreatment conditions, and after transient and stability tests are reported in Fig. 4, and the calculated average Pd particle size is summarized in Table 1. The as prepared $PdAcCeO_2$-M (Fig. 4a) shows highly dispersed Pd species via the absence of any appreciable PdO or Pd(111) patterns. After oxidative pretreatment, on $PdAcCeO_2$-M-o the palladium species remain highly dispersed while, after reduction, on $PdAcCeO_2$-M-h aggregation and considerable sintering occurs, resulting in a Pd particle size of approximately 39 nm (Fig. 4b). Remarkably, the exposure to reaction conditions, either in transient ramp tests (Fig. 4c) or stability tests (Fig. 4d), has little effect on the particle size distribution obtained after the different pretreatments: on $PdAcCeO_2$-M-h, Pd species remain evident on the catalyst surface, with only a partial occurrence of a secondary Pd-C_x phase causing a shift to lower 2θ of the Pd(111) peak due to carbon incorporation [60] after temperature ramp test to 500 °C (Fig. 4c). Conversely, on $PdAcCeO_2$-M-o only mild sintering of palladium species occurs, resulting in an estimated particle size of about 10 nm after transient tests that appears to be stable even after 48 h time-on-stream test at 400 °C. The expanded Pd(111) lattice due to C incorporation is also more significant (Fig. 4c,d), suggesting that it might be involved in the differences in selectivity observed during activity tests. The robust nature of Pd-CeO_2 structure obtained after O_2 treatment is confirmed by the XRD profiles of the $PdAcCeO_2$-M-o-h sample, which closely resemble the patterns collected over the $PdAcCeO_2$-M sample exposed to air only.

To discern the amount and nature of coke which could be deposited on the catalysts surface, as suggested both by activity results and by XRD measurements, complementary thermogravimetric analysis was carried out on the samples after transient and stationary reactivity tests (Fig. S5). On all samples, the weight loss corresponding to carbon residues removal occurs below 250 °C, suggesting that no structured coke is present on either sample [61]. Above 250 °C, oxidation of the metallic Pd species occur and the changes observed at higher temperature (at 800 °C and 700 °C during heating and cooling, respectively) correspond to the release and uptake of O_2 corresponding to the well-known hysteretic decomposition-reoxidation behavior of PdO [62,63]. The anticipated decomposition of PdO and partial oxidation of Pd on $PdAcCeO_2$-M-h confirms the presence of larger particles on the catalyst, while on $PdAcCeO_2$-M-o and M-o-h a better dispersion of palladium species is maintained throughout reaction, as demonstrated by the more facile Pd↔PdO hysteretic behavior [64], i.e., the full re-oxidation observed on these samples while only a partial closing of the hysteresis is observed on the M-h catalyst (Fig. S5a,b).

Therefore, from TGA and XRD characterization we can infer that, in general, a minimal amount of C_x or C_xH_y fragments accumulate on the catalysts surface, in line with their presence in Pd particles in a less than stoichiometric (<1) ratio [60], and they likely concur to the different reaction routes enabled for CO_2 activation, similarly to what observed under dry reforming conditions [56].

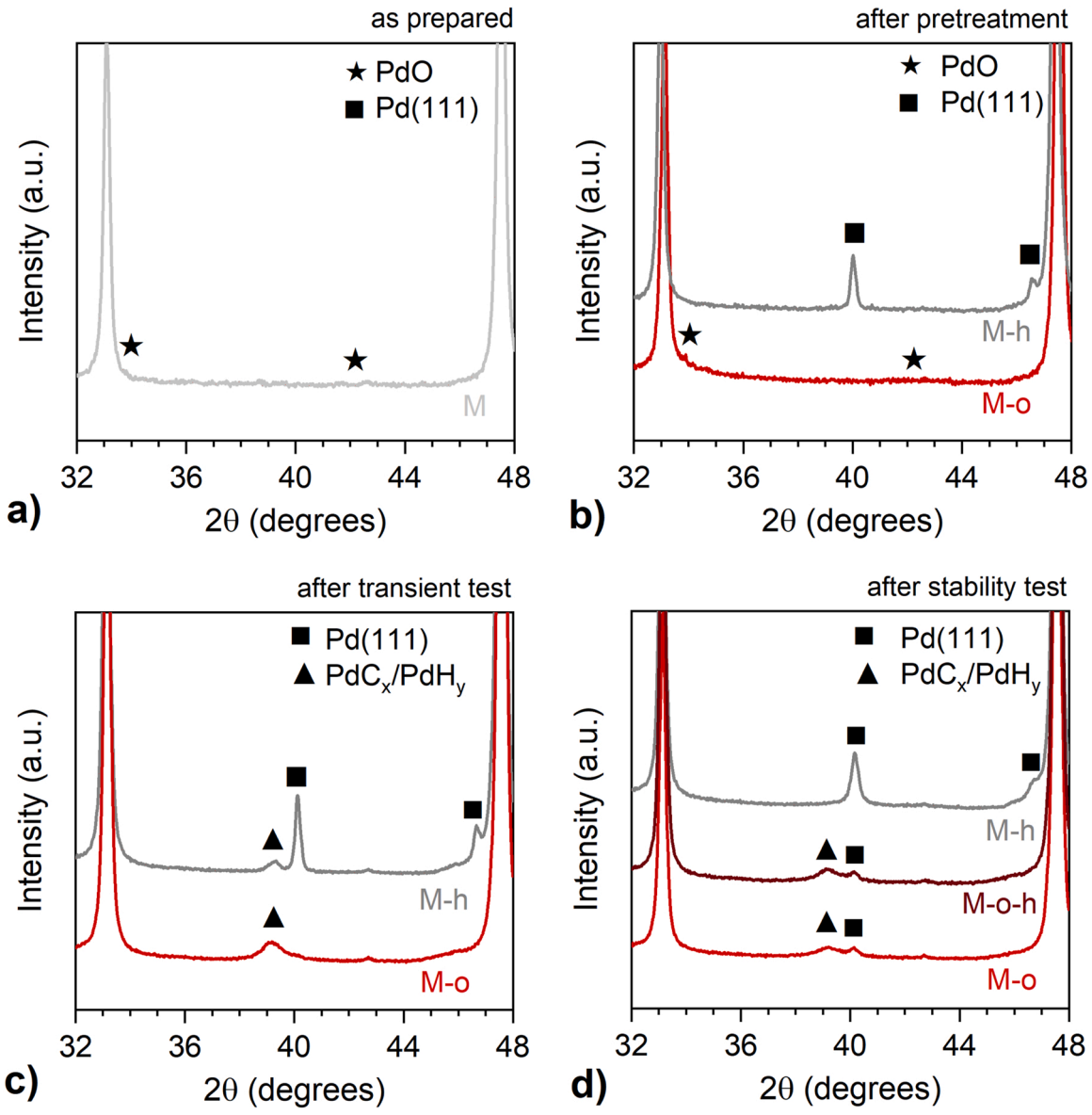

Fig. 4. XRD patterns collected in the Pd-PdO 2θ range on PdAcCeO$_2$-M: (a) as prepared, (b) after oxidative and reducing pretreatment, (c) after transient CO_2 hydrogenation test up to 500 °C, and (d) after stability test for 48 h at 400 °C.

Table 1
Estimated Pd particle size on PdAcCeO$_2$-M after pretreatment, transient and stability experiments.

Pretreatment atmosphere	Average Pd particle size (nm)		
	After pretreatment	After transient test	After stability test
O_2	n.a.[a]	10	11
H_2	39	39	27
O_2-H_2	–	–	14

[a] PdO peak too small for detection.

3.3. DRIFTS studies

To further explore the difference in CO_2 hydrogenation activity, *in situ* DRIFTS under identical reaction conditions was used to discern the surface species that may account for the observed differences in selectivity (Fig. 5). At 400 °C, where the oxidative vs. reducing treatment leads to the largest difference in selectivity, DRIFTS analysis highlights a very different surface environment: two distinct linear Pd-CO peaks at 2060 and 2033 cm^{-1} and a bridged Pd-CO site at 1942 cm^{-1} appear on PdAcCeO$_2$-M-o, while no Pd-CO binding is observed after H_2 reduction (Fig. 5a). Moreover, PdAcCeO$_2$-M-o lacks the 1420 cm^{-1} band, attributed to monodentate carbonate, presenting instead a higher intensity carbonate band at 1280 cm^{-1}, while both samples show formate bands at 1595 cm^{-1} (Fig. 5b). At 250 °C, where both conditions result in 100% selectivity towards CO, the spectra are uniform in the carbonate region, showing formates (HCOO) at 1590, 1395, and 1370 cm^{-1} and carbonates (HCO_3^-) at 1330 and 1282 cm^{-1}, with no peak shifting on any of the positions for either catalyst or pretreatment condition (Fig. S6). The difference in carbonyl formation over PdAcCeO$_2$-M-o relative to PdAcCeO$_2$-M-h is not solely due to differences in particle size, because larger particles would still result in bridged or hollow Pd-CO sites. Similar observations with regards to Pd-CO on PdAcCeO$_2$-M at high temperature was also observed during methane dry reforming, where the CO_2 reduction was believed to contribute to the formation of the Pd-CO intermediates [56]. Therefore, the unique moieties generated by the oxidative treatment result in both a decrease in particle size, evidenced by XRD, and additionally exposes distinct Pd-CO atop sites, which are lacking over the catalyst exposed to a reductive treatment.

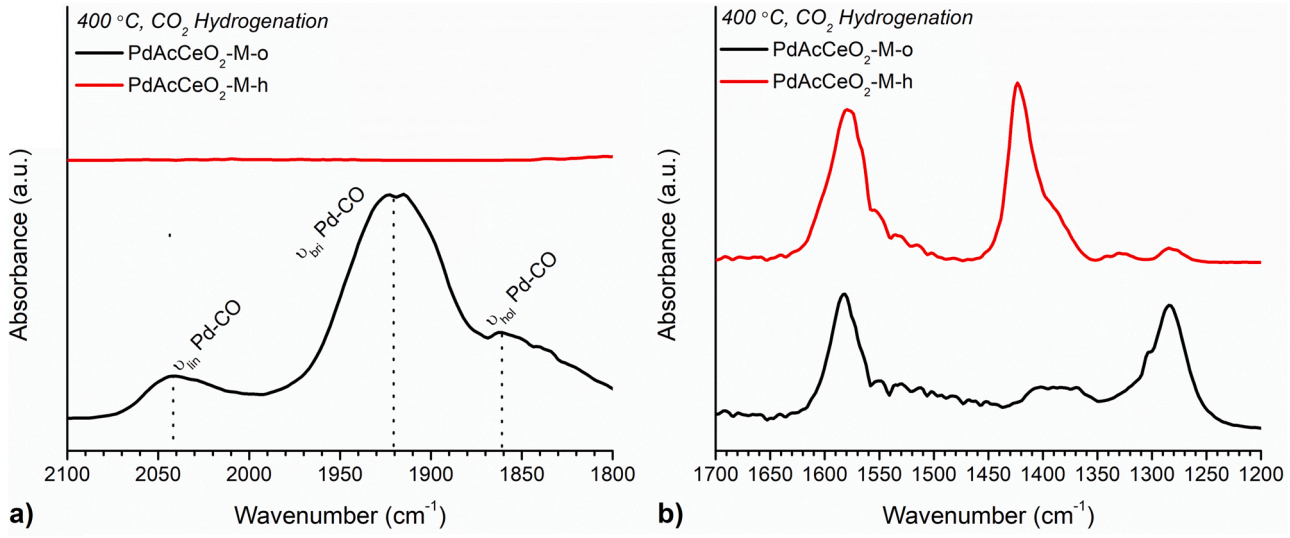

Fig. 5. *In situ* CO_2 hydrogenation DRIFTS for the corresponding $PdCeO_2$ catalysts at 400 °C in the (a) CO_{ads} region and (b) carbonate region. Conditions: 4:1:95 H_2:CO_2:N_2, 1 atm pressure, MCT detector, 4 cm^{-1} resolution.

To rule out the contribution from CO_2 adsorption on the surface species, the spectra at the same temperature and pretreatment conditions were collected under a comparable 1% CO_2/He atmosphere, shown in Fig. S7. The CO_2 adsorption shows that upon pretreatment in a reducing environment, $PdAcCeO_2$-M-h, CO_2 adsorbs as a formate species at 250 °C, while for the oxidative treatment there are only carbonates at ~1400 cm^{-1} and 1280 cm^{-1}. This is possibly due to residual Pd hydrides from the pretreatment partially hydrating adsorbed CO_2 into formate [59]. At 400 °C (Fig. S7b) the CO_2 adsorption spectra for both conditions appear identical, likely due to the fact the surface has stabilized at the elevated temperature and there is an absence of the initial saturation of hydrogen [65]. Pure CO_2 adsorption in the absence of H_2 is not expected to strongly bind to the Pd surface at high temperatures, instead favoring binding to the supporting material [66], in this case CeO_2 which results in weakly bound surface species and signal. Thus, the immediate difference between the two catalysts is the preferential formation of carbonyl intermediates (2200–1800 cm^{-1}) under reaction conditions, specifically linear Pd-CO (2040 cm^{-1}), bridged Pd-CO (1920 cm^{-1}) and hollow Pd-CO (1860 cm^{-1}), which was absent over stoichiometric CO_2 adsorption at 400 °C. This suggests that $PdAcCeO_2$-M-o has a higher affinity for the dissociation of CO_2 into CO, therefore saturating the Pd surface, while $PdAcCeO_2$-M-h does not yield any Pd-CO species under CO_2 hydrogenation conditions (Fig. 5a). Based on the *in situ* CO_2 hydrogenation DRIFTS at both 250 °C and 400 °C coupled with the non-catalytic adsorption of CO_2 to probe its static adsorption on the surface, we can clearly observe that the formate band is consistent across all catalysts, where formate is generally considered to be a favorable intermediate species for RWGS and subsequent methanol synthesis [13,28,59], not methanation [19,67,68], while the absence of monodentate carbonate suggests that this species is being consumed via an associate mechanism of HCOO hydrogenation. Furthermore, on $PdAcCeO_2$-M-o formate species readily desorb under He at reaction conditions in under one minute, showing they are not strongly bound to the surface, while for $PdAcCeO_2$-M-h the formate species remain on the surface for over five minutes, showing they are too strongly bound to $PdAcCeO_2$-M-h and are likely spectators on the pre-reduced samples (Fig. S8).

To explore the observed increase in methane yield after cycling between reductive and oxidative treatments over $PdAcCeO_2$-M, we carried out similar cycling experiments while monitoring the surface species via DRIFTS, as shown in Fig. 6. The 1st cycle is after an initial oxidative treatment, the 2nd cycle is after a reductive treatment while the 3rd is after an oxidative treatment following the same treatment conditions as done for the reactivity measurements. While the overall surface species are not affected in terms of their identity, their relative population changes upon each cycling step. After a reductive treatment, the concentration of Pd-CO carbonyl groups (2100–1800 cm^{-1}) on the surface is decreased relative to the total carbonate species concentration, where Kubelka-Munk IR account for relative surface concentration, and a clear shifting of Pd-CO hollow sites from 1880 cm^{-1} to 1885 cm^{-1} is observed, indicating particle sintering. After a secondary oxidative treatment, the concentration of carbonyls increases again relative to the total concentration of carbonates, while the trend of a blue shifting of the Pd-CO hollow sites is observed, moving the Pd-CO hollow site to ~1890 cm^{-1}. Moreover, after a secondary oxidative treatment additional carbonate species are observed at 1540 cm^{-1} which were not present after both the initial cycle and the second reductive cycle.

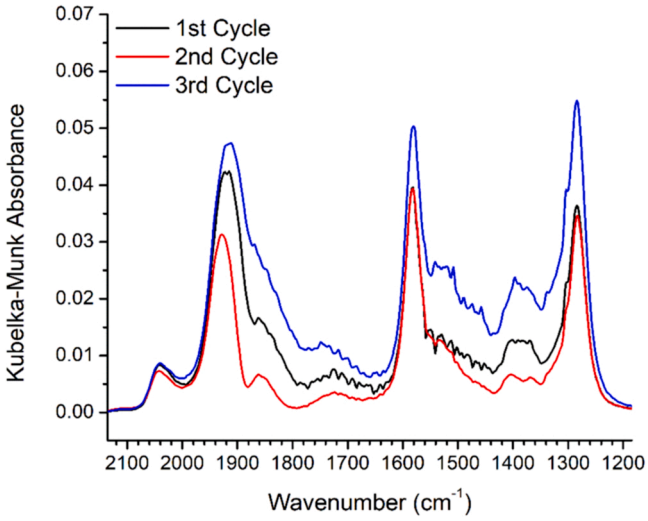

Fig. 6. CO_2 hydrogenation DRIFTS over $PdAcCeO_2$-M-o-h at steady state after different pretreatments. 1st cycle treatment: 450 °C under 20%O_2/He for 1 h, 2nd cycle: 400 °C under 4%H_2/He for 30 min and 3rd cycle: 450 °C under 20% O_2/He for 1 h. All spectra collected at 400 °C under 1%CO_2 4%H_2 balance He with 50 mL/min total flow, 4 cm^{-1} resolution, 1 atm pressure.

To probe the contribution from the immediate CO_2 dissociative mechanism, which generally occurs on the surface of the metal forming

a carbonyl [3,17], and the associative mechanism of CO_2 hydrogenation, which would likely occur at the interfacial metal-support sites [13,14,66], a simulated CO_2 dissociation was modeled in Fig. 7: by feeding a gas composition of 3:1 H_2:CO, we are essentially modeling CO_2 hydrogenation after the initial H_2 is used solely for the RWGS step to produce CO_{ads} and CO (g), effectively simulating a pure CO_2 dissociative mechanism. From this we can observe that the surface chemistry of PdAcCeO$_2$-M-o is largely unchanged in the presence of either CO or CO_2 hydrogenation, which suggests that PdAcCeO$_2$-M-o is not rate limited by the dissociation of CO_2. Furthermore, over PdAcCeO$_2$-M-h we see a similar consistency in that the surface is covered almost exclusively by carbonates and no Pd-CO, even in the case of CO hydrogenation. The absence of Pd-CO peaks over PdAcCeO$_2$-M-h suggests that the CO is reacting sufficiently fast such that there is no observable CO adsorbed, with the exception of a broad Pd-CO hollow feature at ~1820 cm^{-1} during CO hydrogenation, which indicates that the hollow Pd-CO may be largely inactive. An important similarity between both PdAcCeO$_2$-M-o and PdAcCeO$_2$-M-h is that CO hydrogenation, with the exception of the Pd-CO region, results in generally identical carbonate features. Upon further desorption of the CO hydrogenation surface intermediates for both pretreatment conditions, we observed that formate (1595 cm^{-1}) was desorbed almost immediately in the presence of a H_2/He purge while the carbonate species at 1390 cm^{-1} remained on the surface throughout the purging, which shows that this species is largely unreactive. This highlights the difference in the associative mechanism being favored over PdAcCeO$_2$-M-o, where CO_2 hydrogenation under ideal 4:1 H_2:CO_2 conditions yields dampened carbonate bands on PdAcCeO$_2$-M-o and a prominent carbonate band on PdAcCeO$_2$-M-h, which may lead to the observed difference in overall methane yield. An extended IR region showing the C-H stretching in the inset is shown in Fig. S9, where PdAcCeO$_2$-M-o yields C-H stretching from bridged formate at 2830 cm^{-1} [69–71] while PdAcCeO$_2$-M-h shows no CH_4 adsorption. The originating carbon species is likely bicarbonate due to the presence of characteristic bands at 1560 and 1280 cm^{-1}, while polycarbonate species, which are likely spectators and not as reactive, are responsible for the notable band at 1400 cm^{-1} on PdAcCeO$_2$-M-h while possessing only a minor presence on PdAcCeO$_2$-M-o [72,73].

With the following understanding of the reaction mechanism of both full CO_2 methanation and CO hydrogenation as a simulated CO_2 dissociative mechanism, we propose the following mechanism for PdAcCeO$_2$-M-o which follows an associative CO_2 hydrogenation mechanism:

$$CO_2\ (g) + xH_2\ (g) \rightarrow CO_2\ (ad) + 2xH\ (ad) \quad (1)$$

$$CO_2\ (ad) + H\ (ad) \rightarrow HCOO\ (ad) \quad (2)$$

$$HCOO \rightarrow CO\ (ad) + OH\ (ad) \quad (3)$$

$$HCOO\ (ad) + H\ (ad) \rightarrow HCO\ (ad) + OH\ (ad) \quad (4)$$

$$HCO\ (ad) + H\ (ad) \rightarrow H_2CO\ (ad) \quad (5)$$

$$H_2CO\ (ad) + H\ (ad) \rightarrow H_3CO\ (ad) \quad (6)$$

$$H_3CO\ (ad) + 2H\ (ad) \rightarrow CH_4\ (g) + OH\ (ad) \quad (7)$$

$$2OH\ (ad) + 2H\ (ad) \rightarrow 2H_2O\ (g) \quad (8)$$

$$CO\ (ad) \rightarrow CO\ (g) \quad (9)$$

where Eq. (4) is the rate limiting step in this process, which results in formate (1595 cm^{-1}) as a predominant surface species. Subsequent steps (5)-(9) occur rapidly and thus are not observed experimentally where the formation of formyl (HCO, 1690 cm^{-1}) and water (broad peaks centered at 1500 cm^{-1}) are not present in the DRIFTS spectra. Eq. (8) represents the hydration of OH groups to make water, which occurs during the reaction, not necessarily at the end, similarly for CO desorption into CO (g). DFT studies suggest that the mechanism proposed herein is the likely formate pathway to methanation [15,74].

One important difference between CO and CO_2 hydrogenation is the preferential adsorption of CO on Pd sites [25,75] while CO_2 preferentially adsorbs on ceria sites [40]. This suggests that on the milled catalyst after O_2 treatment the reactivity could be promoted by an increased number of interfacial Pd-Ce sites, which would primarily influence CO_2 hydrogenation DRIFTS spectra [76] while leaving CO hydrogenation spectra relatively unaffected, as observed in these simulated CO_2 dissociation experiments. Furthermore, this is corroborated by the redispersion revealed by post reaction XRD analysis, resulting in higher metal-support interfacial active sites.

3.4. Isotopic labeling of CO_2 hydrogenation via in situ DRIFTS

Isotopic labeling via D_2 was applied to further elucidate the reaction mechanism for CO_2 methanation over the PdAcCeO$_2$-M catalysts. To probe the transient dynamics of the reaction, H_2/D_2 were cycled ten times and each cycle of either H_2 or D_2 was allowed to reach steady state, thus effectively probing which surface species were merely spectators and which were actively involved in the reaction. Furthermore, the time

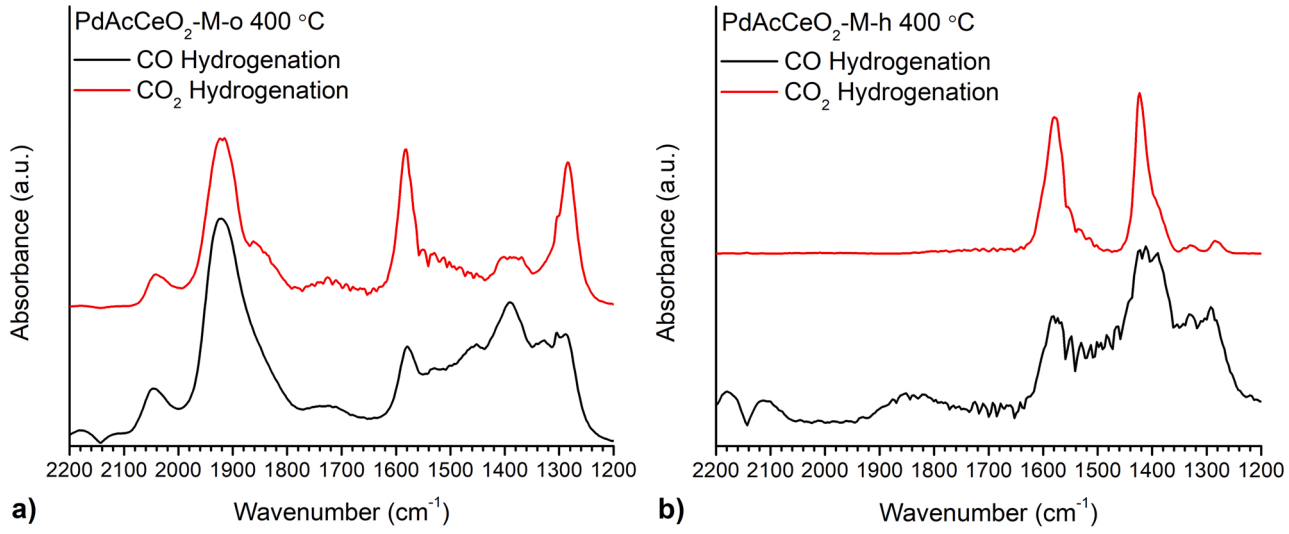

Fig. 7. CO hydrogenation surface species compared against CO_2 hydrogenation DRIFTS for (a) PdAcCeO$_2$-M-o and (b) PdAcCeO$_2$-M-h Conditions: CO hydrogenation 3:1:96 ratio of H_2:CO:He or CO_2 hydrogenation 4:1:95 ratio of H_2:CO_2:He, 50 mL/min total flow, 4 cm^{-1} resolution, MCT detector.

resolution for the spectra acquisition was 7 s, which allows us to capture the true transient species with a minimal dead volume during gas switching. These findings are shown in Fig. 8 for PdAcCeO$_2$-M-o, which had a richer surface chemistry than PdAcCeO$_2$-M-h, where the measurements were under analogous conditions to the reactivity measurements at 400 °C and 1 atm pressure, shown in Figs. 1 and 2. Immediately, one can see that the isotopic switching results in loss of CH_4 at 3015 cm^{-1} in favor of CD_4 at 2264 cm^{-1}, indicating that the isotope substitution is resulting in successful turnovers of methane. The formate and carbonate C-O region between 1000 and 1800 cm^{-1} shows little change, however, the bands in this region are composed primarily of O-C-O bonding which are not expected to change dramatically via the substitution of H/D. The most notable substitution is in the C-H region between 2500 and 2800 cm^{-1}, which shows immediate uptake of deuterium into the mechanism. Specifically, the peaks at 2690 cm^{-1} and 2790 cm^{-1} are caused by the C-D substitution of the formate species [77, 78]. The broad band centered at ~2600 cm^{-1} is due to the -OD surface groups that are substituted in the presence of D_2 as a reductant, which show that surface -OH/-OD groups are contributing to the reaction mechanism, likely as CO_2 adsorbing sites on ceria. Upon reaction of the oxygen vacancies and subsequent oxygen replenishment, surface OD groups are expected to form in a system with an active and reducible supporting material. Furthermore, the cycling uptake of D_2 is incredibly reproducible, where the H_2/D_2 was repeated over twenty times and each cycle was perfectly repeated. This shows that the surface cycling is not an artifact but actually contributing to the reaction mechanism, as a spectator would yield a time delay in the measurement, which is not the case for PdAcCeO$_2$-M-o. The isotopic measurements are consistent with the mechanism provided in Eqs. (1)–(9), where there is clear C-D exchange consistent with HCOO being the rate determining step, Eq. (4), and an abundance of surface OD as a result of the reaction mechanism and the production of water. Therefore, the modified reaction equations verified via isotopic labeling are as follows:

$$CO_2\ (g) + xD_2\ (g) \rightarrow CO_2\ (ad) + 2xD\ (ad) \quad (10)$$

$$CO_2\ (ad) + D\ (ad) \rightarrow DCOO\ (ad) \quad (11)$$

$$DCOO \rightarrow CO\ (ad) + OD\ (ad) \quad (12)$$

$$DCOO\ (ad) + D\ (ad) \rightarrow DCO\ (ad) + OD\ (ad) \quad (13)$$

$$D_3CO\ (ad) + 2D\ (ad) \rightarrow CD_4\ (g) + OD\ (ad) \quad (14)$$

$$2OD\ (ad) + 2D\ (ad) \rightarrow 2D_2O\ (g) \quad (15)$$

Where CD_4 was immediately observed in addition to D-C stretching and broad OD bands. This also shows that the OH recombination with surface D (ad) to form D_2O is also not necessarily spontaneous as the OD species are clearly observed in the deuterated spectra.

3.5. Evaluation of the surface electronic state via AP-XPS

To implement the findings of the *in situ* DRIFTS we employed ambient pressure XPS (AP-XPS) to directly link the changes in the adsorbed surface species to the chemical speciation of palladium. The Pd*3d* and Ce*3d* regions were collected under UHV after pretreatment in either H_2 or O_2 from room temperature to 400 °C under 30 mtorr of a 4:1 ratio of H_2:CO_2 to discern the surface chemical structure under reaction conditions (Figs. S10 and S11, respectively). All spectra were calibrated to Ce*3d* Ce^{4+} at 916.9 eV [40]. The Pd*3d* spectra for room temperature PdAcCeO$_2$-M-o and PdAcCeO$_2$-M-h show the state of the Pd immediately after pretreatment, highlighting a more oxidized Pd^{4+}/Pd^{2+} mixture on the former and fully reduced Pd^0 on the latter. At 250 °C, the Pd surface compositions over both PdAcCeO$_2$-M-o and PdAcCeO$_2$-M-h are analogous, presenting mainly Pd^0 species, consistent with DRIFTS and reactivity measurements at 250 °C. The spectra of the catalysts after different pretreatment conditions are compared against each other at

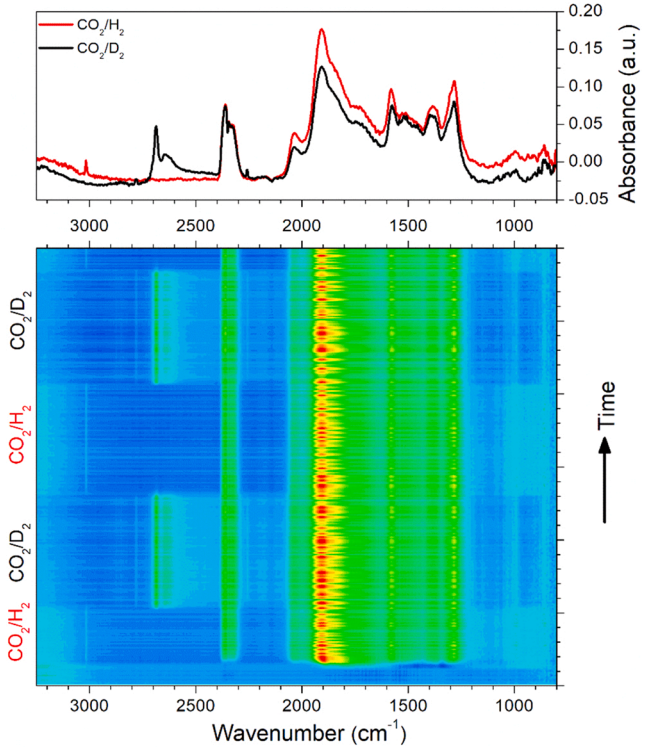

Fig. 8. Isotopic switching of CO_2/H_2 and CO_2/D_2 over PdAcCeO$_2$-M-o. Spectra initiated in CO_2/H_2 at t = 0 s, and subsequently switched back and forth from H_2 to D_2; top spectra representative of steady state CO_2/H_2 and CO_2/D_2 scans.

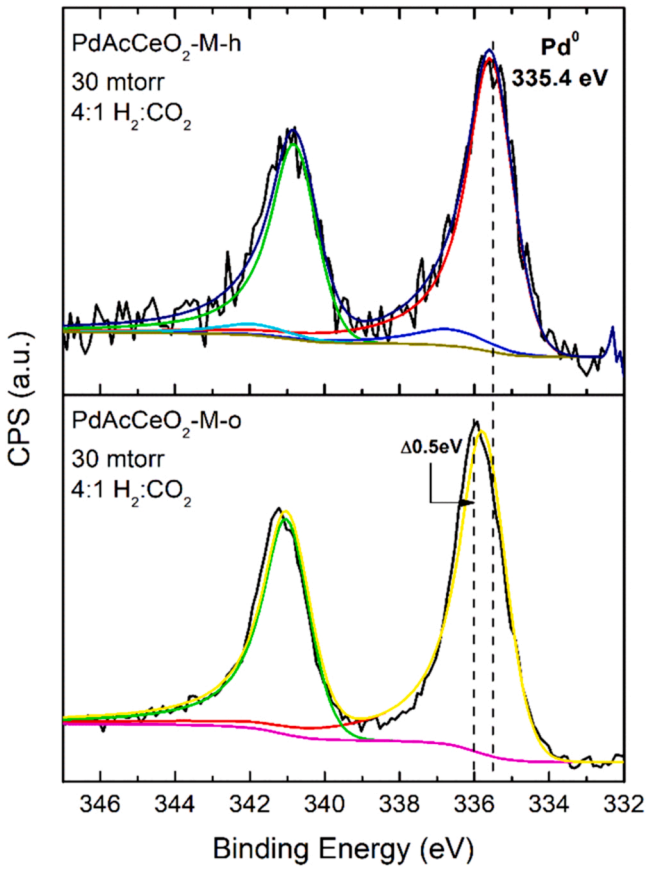

Fig. 9. AP-XPS of Pd3d region at 400 °C for PdAcCeO$_2$-M after varied pretreatment conditions. *in situ* conditions: 30 mtorr 4:1 H_2:CO_2.

400 °C in Fig. 9, corresponding to the most significant difference in selectivity. At 400 °C, a clear difference in the Pd*3d* region can be observed for the $PdAcCeO_2$-M-o catalyst, which results in the formation of a distinct $Pd^{\delta+}$-C modified species at 335.9 eV while $PdAcCeO_2$-M-h shows both the formation of Pd^{2+} at 336.8 eV and only Pd^0 at 335.4 eV and the absence of the shifted $Pd^{\delta+}$ species. The Pd^{2+}, generated via oxidation via water under reaction conditions, slightly increases in the case of $PdAcCeO_2$-M-h due to the elevated temperature increasing the rate of water generation via the RWGS, while it decreases on $PdAcCeO_2$-M-o, where only $Pd^{\delta+}$ species appear at 400 °C.

The formation of a surface overlayer of Pd-C_x is corroborated by the post reaction XRD for $PdAcCeO_2$-M-o, which shows a partial formation of PdC_x species adjacent to the primary metallic Pd diffraction. A similar formation of Pd-C species was found to occur over these catalysts under DRM reaction conditions [56]. The surface sensitivity of AP-XPS has a bias to overrepresent the surface, and PdC_x, clearly observed in bulk diffraction, is expected to begin forming on the outer layer of the Pd nanoparticle, as CO_2 is the primary source of carbon deposition and is expected to diffuse into Pd from its outer surface radially inwards. However, while the carbon diffusion into the Pd particle is incomplete, shown by the parallel Pd^0/PdC_x diffraction peaks via XRD, it is sufficient to saturate the surface species which are the most catalytically relevant and captured via AP-XPS, specifically for $PdAcCeO_2$-M-o. The presence of carbon modified Pd may be correlated to the differences in surface species observed via DRIFTS and the factor of two higher methane yield relative to $PdAcCeO_2$-M-h, all of which occurs exclusively at 400 °C. The Ce*3d* spectra for $PdAcCeO_2$-M-o and $PdAcCeO_2$-M-h at all temperatures at 30mtorr pressure (Fig. S12) show little change in the surface composition of CeO_2 after initial exposure to the reaction gas mixture. This indicates there is little contribution from the lattice oxygen on the CO_2 hydrogenation reaction for these catalysts.

4. Conclusions

The reactivity of $PdAcCeO_2$ milled catalysts under CO_2 hydrogenation conditions was investigated following the kinetics, surface species, and surface composition of the catalysts via several spectroscopic and textural techniques, in order to elucidate the different reaction mechanisms enabled by the unique Pd-Ce interaction promoted by the mechanical synthesis route. Remarkably, a H_2 or O_2 pretreatment atmosphere showed a significant effect in tuning the reaction selectivity towards CO or CH_4 production, respectively. The oxidative treatment proved to lead to a robust catalytic activity, maintained even under prolonged exposure to reducing reaction conditions carried out in the stoichiometric 1:4 CO_2:H_2 ratio, demonstrating stable CH_4 selectivity and minor deactivation over 50 h time-on-stream tests.

By means of *in situ* and isotopic labeling DRIFTS, unique monodentate carbonate surface species and the formation of stable Pd-CO species were detected on the $PdAcCeO_2$-M-o catalyst, while carbonate species were observed at low temperature and on $PdAcCeO_2$-M-h after H_2 treatments, where selectivity to CO is predominant. DRIFTS results suggest that the methanation reaction proceeds via a CO_2 associative pathway on $PdAcCeO_2$-M-o, possibly promoted by the larger availability of Pd-Ce interfacial sites, while on the $PdAcCeO_2$-M-h sample the RWGS CO_2 dissociation pathway is favored. In parallel, the $PdAcCeO_2$-M structure and the surface electronic states obtained after various pretreatments were probed by means of XRD and AP-XPS analyses, respectively. This highlighted a mixed modified $Pd^{\delta+}$-C state on the $PdAcCeO_2$-M-o catalyst at 400 °C under reaction conditions shifting the Pd^0 binding energy from 335.4 eV to approximately 336 eV. Likely, C species from CO_2 hydrogenation diffuse into Pd^0 particles, affecting CO adsorption over the $Pd^{\delta+}$-C overlayer and tuning the reaction pathway towards CO_2 adsorption and its associative reduction to CH_4 at the Pd-Ce interface, which together with the carbon-modified $Pd^{\delta+}$ species also plays a key role in promoting the direct methanation of CO_2.

The facile tuning of CO_2 selectivity on $PdAcCeO_2$-M by mild treatments allowed us to analyze the different reaction intermediates and Pd states involved in the CO vs CH_4 production, opening new pathways for the design of Pd/CeO_2 based CO_2 hydrogenation catalysts, where the reactivity can be easily tuned depending on the desired reaction products and could be of potential interest as materials for carbon dioxide conversion in O_2-rich streams.

CRediT authorship contribution statement

M.D. and J.D.J carried out the experiments, wrote the manuscript and conceived the project. N.R., J.M., and L.E.B. helped in data acquisition. A.T. and J.A.R. provided oversight and insights into manuscript. S.D.S and S.C oversaw entirety of project, funding, conceptualization, and manuscript preparation. All authors contributed to the final drafting of the manuscript.

Declaration of Competing Interest

The authors declare that they have no known competing financial interests or personal relationships that could have appeared to influence the work reported in this paper.

Data availability

Data will be made available on request.

Acknowledgments

M.D. is grateful for funding under the REACT EU Italian PON 2014–2020 Program – Action IV.4 – Innovation (DM 1062, 10/08/2021) and under the Fondazione CRUI “Go for IT” Program. A.T. acknowledges the Interconnected Nord-Est Innovation Ecosystem (iNEST) and received funding from the European Union Next-GenerationEU (Piano Nazionale di Ripresa e Resilienza (PNRR) – Missione 4 Componente 2, Investimento 1.5 – D.D. 1058 23/06/2022, ECS00000043). This manuscript reflects only the authors’ views and opinions, neither the European Union nor the European Commission can be considered responsible for them. The work carried out at Brookhaven National Laboratory was supported by the US Department of Energy under contract no. DE-SC0012704. S.D.S. is supported by a US Department of Energy Early Career Award.

Appendix A. Supplementary material

Supplementary data associated with this article can be found in the online version at doi:10.1016/j.apcata.2023.119185.

References

[1] M.A.A. Aziz, A.A. Jalil, S. Triwahyono, A. Ahmad, Green Chem. 17 (2015) 2647–2663.
[2] M.N. Anwar, A. Fayyaz, N.F. Sohail, M.F. Khokhar, M. Baqar, A. Yasar, K. Rasool, A. Nazir, M.U.F. Raja, M. Rehan, M. Aghbashlo, M. Tabatabaei, A.S. Nizami, J. Environ. Manag. 260 (2020), 110059.
[3] S. Saeidi, S. Najari, V. Hessel, K. Wilson, F.J. Keil, P. Concepción, S.L. Suib, A. E. Rodrigues, Prog. Energy Combust. Sci. 85 (2021), 100905.
[4] M. Wang, L. Luo, C. Wang, J. Du, H. Li, J. Zeng, Acc. Mater. Res. 3 (2022) 565–571.
[5] Z. Zhang, S.-Y. Pan, H. Li, J. Cai, A.G. Olabi, E.J. Anthony, V. Manovic, Renew. Sustain. Energy Rev. 125 (2020), 109799.
[6] H. Arakawa, M. Aresta, J.N. Armor, M.A. Barteau, E.J. Beckman, A.T. Bell, J. E. Bercaw, C. Creutz, E. Dinjus, D.A. Dixon, K. Domen, D.L. DuBois, J. Eckert, E. Fujita, D.H. Gibson, W.A. Goddard, D.W. Goodman, J. Keller, G.J. Kubas, H. H. Kung, J.E. Lyons, L.E. Manzer, T.J. Marks, K. Morokuma, K.M. Nicholas, R. Periana, L. Que, J. Rostrup-Nielson, W.M.H. Sachtler, L.D. Schmidt, A. Sen, G. A. Somorjai, P.C. Stair, B.R. Stults, W. Tumas, Chem. Rev. 101 (2001) 953–996.
[7] Y. Guo, Z. Liu, F. Zhang, D.-J. Wang, K. Yuan, L. Huang, H.-C. Liu, S.D. Senanayake, J.A. Rodriguez, C.-H. Yan, Y.-W. Zhang, ChemCatChem 13 (2021) 874–881.
[8] P. Panagiotopoulou, Appl. Catal. A Gen. 542 (2017) 63–70.
[9] A. Aitbekova, L. Wu, C.J. Wrasman, A. Boubnov, A.S. Hoffman, E.D. Goodman, S. R. Bare, M. Cargnello, J. Am. Chem. Soc. 140 (2018) 13736–13745.

[10] J.C. Matsubu, V.N. Yang, P. Christopher, J. Am. Chem. Soc. 137 (2015) 3076–3084.
[11] C. Shen, K. Sun, R. Zou, Q. Wu, D. Mei, C. Liu, ACS Catal. 12 (2022) 12658–12669.
[12] A. Parastaev, V. Muravev, E.H. Osta, T.F. Kimpel, J.F.M. Simons, A.J.F. van Hoof, E. Uslamin, L. Zhang, J.J.C. Struijs, D.B. Burueva, E.V. Pokochueva, K.V. Kovtunov, I.V. Koptyug, I.J. Villar-Garcia, C. Escudero, T. Altantzis, P. Liu, A. Béché, S. Bals, N. Kosinov, E.J.M. Hensen, Nat. Catal. 5 (2022) 1051–1060.
[13] T. Chen, C. Cao, T. Chen, X. Ding, H. Huang, L. Shen, X. Cao, M. Zhu, J. Xu, J. Gao, Y.-F. Han, ACS Catal. 9 (2019) 8785–8797.
[14] B. Yan, B. Zhao, S. Kattel, Q. Wu, S. Yao, D. Su, J.G. Chen, J. Catal. 374 (2019) 60–71.
[15] S. Kattel, P. Liu, J.G. Chen, J. Am. Chem. Soc. 139 (2017) 9739–9754.
[16] L.R. Winter, R. Chen, X. Chen, K. Chang, Z. Liu, S.D. Senanayake, A.M. Ebrahim, J. G. Chen, Appl. Catal. B Environ. 245 (2019) 360–366.
[17] C. Vogt, E. Groeneveld, G. Kamsma, M. Nachtegaal, L. Lu, C.J. Kiely, P.H. Berben, F. Meirer, B.M. Weckhuysen, Nat. Catal. 1 (2018) 127–134.
[18] G.D. Weatherbee, C.H. Bartholomew, J. Catal. 77 (1982) 460–472.
[19] J.D. Jimenez, C. Wen, J. Lauterbach, Catal. Sci. Technol. 9 (2019) 1970–1978.
[20] J.D. Jimenez, C. Wen, M.M. Royko, A.J. Kropf, C. Segre, J. Lauterbach, ChemCatChem 12 (2020) 846–854.
[21] G. Melaet, W.T. Ralston, C.-S. Li, S. Alayoglu, K. An, N. Musselwhite, B. Kalkan, G. A. Somorjai, J. Am. Chem. Soc. 136 (2014) 2260–2263.
[22] T. Abe, M. Tanizawa, K. Watanabe, A. Taguchi, Energy Environ. Sci. 2 (2009) 315–321.
[23] M. Fan, J.D. Jimenez, S.N. Shirodkar, J. Wu, S. Chen, L. Song, M.M. Royko, J. Zhang, H. Guo, J. Cui, K. Zuo, W. Wang, C. Zhang, F. Yuan, R. Vajtai, J. Qian, J. Yang, B.I. Yakobson, J.M. Tour, J. Lauterbach, D. Sun, P.M. Ajayan, ACS Catal. 9 (2019) 10077–10086.
[24] J.H. Kwak, L. Kovarik, J. Szanyi, ACS Catal. 3 (2013) 2094–2100.
[25] L. Fan, J. Zhang, K. Ma, Y. Zhang, Y.-M. Hu, L. Kong, A. Jia, Z. Zhang, W. Huang, J.-Q. Lu, J. Catal. 397 (2021) 116–127.
[26] Y. Lou, F. jiang, W. Zhu, L. Wang, T. Yao, S. Wang, B. Yang, B. Yang, Y. Zhu, X. Liu, Appl. Catal. B Environ. 291 (2021), 120122.
[27] J. Graciani, K. Mudiyanselage, F. Xu, A.E. Baber, J. Evans, S.D. Senanayake, D. J. Stacchiola, P. Liu, J. Hrbek, J.F. Sanz, J.A. Rodriguez, Science 345 (2014) 546–550.
[28] S. Kattel, P.J. Ramírez, J.G. Chen, J.A. Rodriguez, P. Liu, Science 355 (2017) 1296–1299.
[29] C. Baltes, S. Vukojević, F. Schüth, J. Catal. 258 (2008) 334–344.
[30] J. Ding, L. Huang, W. Gong, M. Fan, Q. Zhong, A.G. Russell, H. Gu, H. Zhang, Y. Zhang, R. Ye, J. Catal. 377 (2019) 224–232.
[31] L. Zhong, F. Yu, Y. An, Y. Zhao, Y. Sun, Z. Li, T. Lin, Y. Lin, X. Qi, Y. Dai, L. Gu, J. Hu, S. Jin, Q. Shen, H. Wang, Nature 538 (2016) 84–87.
[32] G. Liu, P. Poths, X. Zhang, Z. Zhu, M. Marshall, M. Blankenhorn, A.N. Alexandrova, K.H. Bowen, J. Am. Chem. Soc. 142 (2020) 7930–7936.
[33] M.S. Frei, C. Mondelli, R. García-Muelas, K.S. Kley, B. Puértolas, N. López, O. V. Safonova, J.A. Stewart, D. Curulla Ferré, J. Pérez-Ramírez, Nat. Commun. 10 (2019) 3377.
[34] J.-N. Park, E.W. McFarland, J. Catal. 266 (2009) 92–97.
[35] Q. Sun, X. Fu, R. Si, C.-H. Wang, N. Yan, ChemCatChem 11 (2019) 5093–5097.
[36] C. Huang, Z. Wu, H. Luo, S. Zhang, Z. Shao, H. Wang, Y. Sun, ACS Appl. Energy Mater. 4 (2021) 9258–9266.
[37] D.J. Pettigrew, D.L. Trimm, N.W. Cant, Catal. Lett. 28 (1994) 313–319.
[38] G. Vilé, D. Albani, M. Nachtegaal, Z. Chen, D. Dontsova, M. Antonietti, N. López, J. Pérez-Ramírez, Angew. Chem. Int. Ed. 54 (2015) 11265–11269.
[39] N. Elia, J. Estephane, C. Poupin, B. El Khoury, L. Pirault-Roy, S. Aouad, E.A. Aad, ChemCatChem 13 (2021) 1559–1567.
[40] Z. Liu, F. Zhang, N. Rui, X. Li, L. Lin, L.E. Betancourt, D. Su, W. Xu, J. Cen, K. Attenkofer, H. Idriss, J.A. Rodriguez, S.D. Senanayake, ACS Catal. 9 (2019) 3349–3359.
[41] J. Jones, H. Xiong, A.T. DeLaRiva, E.J. Peterson, H. Pham, S.R. Challa, G. Qi, S. Oh, M.H. Wiebenga, X.I. Pereira Hernandez, Y. Wang, A.K. Datye, Science 353 (2016) 150–154.
[42] M. Cargnello, V.V.T. Doan-Nguyen, T.R. Gordon, R.E. Diaz, E.A. Stach, R.J. Gorte, P. Fornasiero, C.B. Murray, Science 341 (2013) 771–773.
[43] D. Vovchok, C. Zhang, S. Hwang, L. Jiao, F. Zhang, Z. Liu, S.D. Senanayake, J. A. Rodriguez, ACS Catal. 10 (2020) 10216–10228.
[44] L. Lin, C.A. Gerlak, C. Liu, J. Llorca, S. Yao, N. Rui, F. Zhang, Z. Liu, S. Zhang, K. Deng, C.B. Murray, J.A. Rodriguez, S.D. Senanayake, J. Energy Chem. 61 (2021) 602–611.
[45] C. Xu, S. De, A.M. Balu, M. Ojeda, R. Luque, Chem. Commun. 51 (2015) 6698–6713.
[46] R.A. Buyanov, V.V. Molchanov, V.V. Boldyrev, Catal. Today 144 (2009) 212–218.
[47] M. Danielis, S. Colussi, C. deLeitenburg, L. Soler, J. Llorca, A. Trovarelli, Angew. Chem. Int. Ed. 57 (2018) 10212–10216.
[48] N.J. Divins, A. Braga, X. Vendrell, I. Serrano, X. Garcia, L. Soler, I. Lucentini, M. Danielis, A. Mussio, S. Colussi, I.J. Villar-Garcia, C. Escudero, A. Trovarelli, J. Llorca, Nat. Commun. 13 (2022) 5080.
[49] A. Toso, M. Danielis, C. de Leitenburg, M. Boaro, A. Trovarelli, S. Colussi, Ind. Eng. Chem. Res. 61 (2022) 3329–3341.
[50] V. Šepelák, A. Düvel, M. Wilkening, K.-D. Becker, P. Heitjans, Chem. Soc. Rev. 42 (2013) 7507.
[51] M.J. Muñoz-Batista, D. Rodriguez-Padron, A.R. Puente-Santiago, R. Luque, ACS Sustain. Chem. Eng. 6 (2018) 9530–9544.
[52] A. Kumar, S. Dutta, S. Kim, T. Kwon, S.S. Patil, N. Kumari, S. Jeevanandham, I. S. Lee, Chem. Rev. 122 (2022) 12748–12863.
[53] A.P. Amrute, J. De Bellis, M. Felderhoff, F. Schüth, Chem. Eur. J. 27 (2021) 6819–6847.
[54] H. Schreyer, R. Eckert, S. Immohr, J. deBellis, M. Felderhoff, F. Schüth, Angew. Chem. Int. Ed. 58 (2019) 11262–11265.
[55] M. Danielis, L.E. Betancourt, I. Orozco, N.J. Divins, J. Llorca, J.A. Rodríguez, S. D. Senanayake, S. Colussi, A. Trovarelli, Appl. Catal. B Environ. 282 (2021), 119567.
[56] J.D. Jiménez, L.E. Betancourt, M. Danielis, H. Zhang, F. Zhang, I. Orozco, W. Xu, J. Llorca, P. Liu, A. Trovarelli, J.A. Rodríguez, S. Colussi, S.D. Senanayake, ACS Catal. 12 (2022) 12809–12822.
[57] M. Danielis, N.J. Divins, J. Llorca, L. Soler, X. Garcia, I. Serrano, L.E. Betancourt, W. Xu, J.A. Rodríguez, S.D. Senanayake, S. Colussi, A. Trovarelli, EES Catal 1 (2023) 144–152.
[58] S.D. Senanayake, J. Zhou, A.P. Baddorf, D.R. Mullins, Surf. Sci. 601 (2007) 3215–3223.
[59] M. González-Castaño, B. Dorneanu, H. Arellano-García, React. Chem. Eng. 6 (2021) 954–976.
[60] W. Vogel, J. Phys. Chem. C 115 (2011) 1506–1512.
[61] E. Aneggi, V. Rico-Perez, C. deLeitenburg, S. Maschio, L. Soler, J. Llorca, A. Trovarelli, Angew. Chem. Int. Ed. 54 (2015) 14040–14043.
[62] R.J. Farrauto, J.K. Lampert, M.C. Hobson, E.M. Waterman, Appl. Catal. B Environ. 6 (1995) 263–270.
[63] P. Gélin, M. Primet, Appl. Catal. B Environ. 39 (2002) 1–37.
[64] S. Colussi, A. Trovarelli, E. Vesselli, A. Baraldi, G. Comelli, G. Groppi, J. Llorca, Appl. Catal. A Gen. 390 (2010) 1–10.
[65] X. Wang, H. Shi, J.H. Kwak, J. Szanyi, ACS Catal. 5 (2015) 6337–6349.
[66] L. Proaño, E. Tello, M.A. Arellano-Trevino, S. Wang, R.J. Farrauto, M. Cobo, Appl. Surf. Sci. 479 (2019) 25–30.
[67] S. Kattel, W. Yu, X. Yang, B. Yan, Y. Huang, W. Wan, P. Liu, J.G. Chen, Angew. Chem. Int. Ed. 55 (2016) 7968–7973.
[68] T. Das, G. Deo, Catal. Today 198 (2012) 116–124.
[69] C. Li, Y. Sakata, T. Arai, K. Domen, K. Maruya, T. Onishi, J. Chem. Soc. Faraday Trans. 1 (85) (1989) 1451.
[70] Y. Guo, S. Mei, K. Yuan, D.-J. Wang, H.-C. Liu, C.-H. Yan, Y.-W. Zhang, ACS Catal. 8 (2018) 6203–6215.
[71] T. Rajkumar, A. Sápi, M. Ábel, J. Kiss, I. Szenti, K. Baán, J.F. Gómez-Pérez, Á. Kukovecz, Z. Kónya, Catal. Lett. 151 (2021) 3477–3491.
[72] C. Li, Y. Sakata, T. Arai, K. Domen, K. Maruya, T. Onishi, J. Chem. Soc. Faraday Trans. 1 (85) (1989) 929.
[73] C. Binet, M. Daturi, J.-C. Lavalley, Catal. Today 50 (1999) 207–225.
[74] A.I. Olivos-Suarez, À. Szécsényi, E.J.M. Hensen, J. Ruiz-Martinez, E.A. Pidko, J. Gascon, ACS Catal. 6 (2016) 2965–2981.
[75] D. Ciuparu, A. Bensalem, L. Pfefferle, Appl. Catal. B Environ. 26 (2000) 241–255.
[76] Á. Szamosvölgyi, T. Rajkumar, A. Sápi, I. Szenti, M. Ábel, J.F. Gómez-Pérez, K. Baán, Z. Fogarassy, E. Dodony, B. Pécz, S. Garg, J. Kiss, Á. Kukovecz, Z. Kónya, Environ. Technol. Innov. 27 (2022), 102747.
[77] A. Rezvani, A.M. Abdel-Mageed, T. Ishida, T. Murayama, M. Parlinska-Wojtan, R. J. Behm, ACS Catal. 10 (2020) 3580–3594.
[78] R.C. Millikan, K.S. Pitzer, J. Am. Chem. Soc. 80 (1958) 3515–3521.